Separation and Measurement of Diffusion Coefficients of Linear and Circular DNAs by Flow Field-Flow Fractionation

Min-Kuang Liu and J. Calvin Giddings*

Field-Flow Fractionation Research Center, Department of Chemistry, University of Utah, Salt Lake City, Utah 84112

Received October 30, 1992; Revised Manuscript Received March 15, 1993

ABSTRACT: In this paper flow field-flow fractionation (flow FFF), an elution separation method, is utilized to separate and to measure the translational diffusion coefficients D of a variety of linear and both single- and double-stranded circular DNA chains in the molecular weight range $M = (0.4\text{–}4.8) \times 10^6$ Da. Equations for component retention times, band broadening, and resolution are given and compared with experimental results. The tradeoff between resolution and separation speed is discussed and experimentally realized. Overloading studies show that ~1 μg of individual DNAs can be isolated per 10–20-min run; the procedure can be readily automated for repetitive runs. Values of D obtained from retention time measurements are tabulated, and these as well as literature D values (for $M = (0.058\text{–}38) \times 10^6$ Da) are compared with expressions of Kirkwood–Riseman (KR), Mandelkern–Flory (MF), Tirado–Garcia de la Torre (TG), and Yamakawa–Fujii (YF). The predicted Ds of MF agree well with data over the high M range ($(0.4\text{–}38) \times 10^6$ Da), while the rigid-rod equation of TG fits data quite well up to $M = 2 \times 10^6$ Da, an M for which the DNA chains is ~70 times longer than that displaying rigid-rod behavior. We find also that D is reasonably described by the simple form $D = AM^{-b}$ over the 3-decade M range examined. Factors involved in the application of FFF to DNAs with $M > 10^7$ Da are discussed including shear degradation, transition to a steric mechanism of FFF, and use of condensed DNA. Severe overloading effects induced by chain entanglement rendered preliminary attempts unsuccessful, but future prospects for applying FFF to high-M DNA are found favorable.

Introduction

The separation and purification of DNA chains of various lengths and configurations are important in attaining numerous analytical and preparative goals in DNA research and applications.[1-3] Electrophoresis, ultracentrifugation, and chromatography, in multiple forms, have been widely used for this purpose.[4-11] By contrast, field-flow fractionation (FFF), which is an extended family of separation techniques applicable to macromolecular and colloidal materials,[12-16] has been applied to DNA separations in only a few instances (see below). This relative inactivity is understandable in that FFF techniques, although broad in scope, are less fully developed and widely applied than chromatography and electrophoresis, having been first conceptualized in the 1960s[17] rather than early in the century. The dearth of FFF results is unfortunate because FFF has advantages that could make it a valuable laboratory resource complementary to conventional techniques in separating and purifying DNA fragments. In addition, FFF has unique capabilities in the measurement of macromolecular properties such as translational diffusion coefficients, hydrodynamic diameters, molecular masses, densities, and so on.[16,18] Not only are these measurements rapid but they are carried out simultaneously with the separation of the component requiring measurement so that the measurement is not perturbed by contamination.

The FFF techniques are flow-based elution methods like chromatography, but they employ an external field as do sedimentation (centrifugation) and electrophoretic techniques. However, unlike sedimentation and electrophoresis, the external field is applied in a direction *perpendicular* to the separation axis, which is the axis of flow. Thus the external field does not directly drive the separation, but rather it induces differential retention within the flow stream.[19,20] By this action the field takes the place of the stationary phase in chromatographic systems. Thus FFF can be thought of as one-phase chromatography, although technically FFF is in a category distinct from chromatography.[20]

Since differential retention in FFF is governed by an external field rather than by the affinity of a stationary phase, FFF acquires a great deal of flexibility. To begin with, retention can be readily increased or decreased over wide limits by adjustments in the field strength. The carrier liquid (or buffer) has only a secondary effect on retention and can thus be adjusted to virtually any desired composition. The flow conditions can be altered to optimize the separation, providing either increased separation speed or improved resolution depending upon needs. It is a simple matter to collect pure fractions from the outlet stream. In addition, the system can be readily automated for repetitive runs. Finally, the separation process takes place in a thin uniform channel whose theoretical tractability yields a rigorous relationship between retention and the properties of the macromolecule that govern its interaction with the applied field.[12-20] Thus these properties (mass, size, diffusion coefficient, etc.) can be measured in the course of, or independently of, the separation process.

The application of different fields gives rise to different FFF techniques.[14-16] These fields or gradients include sedimentation fields (sedimentation FFF), crossflow (flow FFF), temperature gradients (thermal FFF), and electrical fields (electrical FFF). In this study we utilize flow FFF, the most universal of the FFF techniques. Flow FFF has been applied to molecules (e.g., humic acids) as small as a few nanometers up to particles of 50-μm diameter.[21,22] The principles and theory of flow FFF will be explained below.

Only a few scattered applications of FFF to DNA have been reported. Kirkland et al. used sedimentation FFF for the separation of several DNAs in the 10^6–10^7 Da molecular weight range,[23-26] including the separation of single-stranded φX174 virion from the double-stranded φX174 RF I DNA.[24] They also separated pBR322 and pDM24D from cell lysates[25] and subsequently, using flow FFF, separated two plasmids from one another.[26] Wahl-

* Corresponding author.

0024-9297/93/2226-3576$04.00/0

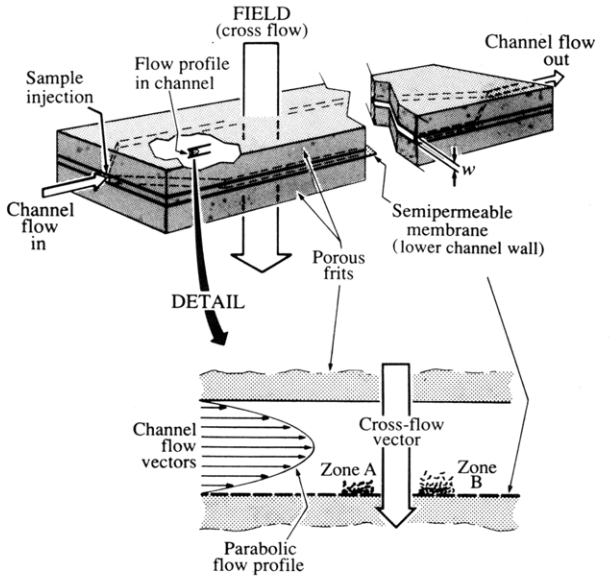

Figure 1. Schematic diagram of the flow FFF channel and separation process.

und and Litzén have separated a number of circular and linear DNAs, some as short as 200 base pairs (bp), using asymmetrical flow FFF.[27,28] More recently, our group demonstrated[29] the flow FFF separation of single-stranded (ϕX174 virion) and double-stranded (ϕX174 RF I) DNA; the separation (shown in Figure 9 of ref 29) was achieved 3 times faster—16 versus 48 min—and with twice the resolution obtained in the sedimentation FFF work cited above.[24]

The above investigations, while useful in demonstrating the applicability of FFF to DNA, have paid only cursory attention to the fundamental behavior of DNA in FFF systems, thus providing very little perspective on the potential range of applicability of FFF, the limitations, and the acquisition of physicochemical constants.

The objectives of the present study are multiple. First, we have expanded the range of applicability of FFF to more diverse forms of DNA. Second, we have extracted a large number of translational diffusion coefficients from the flow FFF retention measurements and correlated these with theoretical diffusion equations. Third, we have investigated overloading phenomena which determine the capacity of FFF for preparative separation. Fourth, we have made a detailed comparison between DNA behavior in flow FFF systems and theoretical expectations, thus providing insights regarding the opportunities and limitations in applying FFF to various types of DNA. Finally, we have examined the opportunities and barriers relating to the possible applications of FFF to very long (>10^7 molecular weight) DNA chains.

Theory of Flow FFF

The principles of flow FFF are illustrated in Figure 1. As the figure shows, flow FFF operates through the superposition of two flow streams, one being the channel flow stream that displaces entrained species along the channel axis toward eventual elution and the other being the crossflow stream that permeates into and through the channel by means of permeable walls. The crossflow stream is directed at right angles to the channel flow stream and has the purpose of driving various components into different transverse distributions in the channel. These distributions occupy different sets of streamlines in the parabolic flow profile of the channel stream. Thus the components are displaced at different velocities and elute at different times. Essential details on this separation mechanism are given below with further elaboration available in prior publications.[21,22,30]

Retention. Because the components being displaced through an FFF channel are driven close to one wall (the accumulation wall) by the crossflow stream, they end up in flow laminae whose velocity is relatively retarded by wall friction compared to that of the average flow lamina. Thus these components are retained relative to an inert marker that samples all flow laminae because of their preferred occupancy of the semistagnant laminae near the wall. The retardation in a component's velocity is represented by the retention ratio R, the mean velocity of the component relative to the mean velocity of an inert tracer. Since velocity is inversely proportional to elution (or retention) time t_r, then $R = t^0/t_r$ where t^0 is the void time (equal to the elution time of an inert marker). According to the standard theory of FFF, R is given by[14,30]

$$R = \frac{t^0}{t_r} = 6\lambda\left(\coth\frac{1}{2\lambda} - 2\lambda\right) \tag{1}$$

in which λ is the retention parameter, a term that can be obtained from[14]

$$\lambda = kT/Fw \tag{2}$$

where k is Boltzmann's constant, T is the absolute temperature, w is the channel thickness, and F is the force exerted by the field on a single particle or macromolecule of the component of interest. For flow FFF this force is given by Stokes' law

$$F = fU = 3\pi\eta dU \tag{3}$$

where d is the hydrodynamic (or Stokes) diameter of the particle, η is the viscosity of the carrier liquid, and U is the velocity of the crossflow stream. The quantity U is related to the flow rate $\dot{V}_c$ of the crossflow stream by[30]

$$U = \dot{V}_c/bL \tag{4}$$

where b is the breadth and L is the length of the channel. The substitution of eqs 3 and 4 into eq 2 shows that λ is inversely proportional to d

$$\lambda = \frac{kTbL}{3\pi\eta\dot{V}_c w}\frac{1}{d} \tag{5}$$

When this expression is substituted into eq 1, a direct relationship is established between the retention time t_r of the component and its hydrodynamic diameter d.

Flow FFF provides the best resolution and speed when $\lambda \ll 1$, a condition induced by a high $\dot{V}_c$. When $\lambda \ll 1$, eq 1 can be approximated by the asymptotic form[14,30]

$$R = t^0/t_r = 6\lambda \tag{6}$$

When eq 5 is substituted into eq 6, the retention time t_r is found to be directly proportional to d

$$t_r = \frac{\pi\eta t^0\dot{V}_c w d}{2kTbL} \tag{7}$$

However, the void time t^0 is simply equal to the void (or channel) volume $V^0 = bLw$ divided by the channel flow rate $\dot{V}$, which leads to

$$t_r = \frac{\pi\eta w^2}{2kT}\frac{\dot{V}_c}{\dot{V}}d \tag{8}$$

This expression relates t_r to known parameters (η, w, and T), to the flow rate ratio $\dot{V}_c/\dot{V}$, and to the hydrodynamic diameter d. Thus a measured value of t_r yields immediately a value for d. The separation of components, which

requires that each has a different t_r is clearly shown by this equation to require different hydrodynamic diameters d.

Alternate expressions can be obtained relating t_r to the friction coefficient f (obtained by using the center term rather than the final term of eq 3) or to the translational diffusion coefficient D through use of the Einstein equation $D = kT/f$. The two relationships are

$$t_r = \frac{w^2}{6kT}\frac{\dot{V}_c}{\dot{V}}f \tag{9}$$

and

$$t_r = \frac{w^2}{6D}\frac{\dot{V}_c}{\dot{V}} \tag{10}$$

The latter can be rearranged into an explicit equation for D

$$D = \frac{w^2}{6t_r}\frac{\dot{V}_c}{\dot{V}} \tag{11}$$

The theoretical relationship between D and t_r was recognized as providing an effective method for measuring D values in some of the earliest work on flow FFF and was applied to proteins, viruses, and latex beads.[30-33]

Equations 7–11 are all simplified expressions based on the asymptotic form of eq 6, which is accurate within 3.5% for $R \leq 0.1$ or 2% for $R \leq 0.06$. However, for numerical calculations we routinely use eq 1 with λ provided by eq 2 and F provided by eq 3, or the equivalent form related to D.

The above equations are applicable when the two flow rates are held constant throughout the run. In some cases $\dot{V}_c$ is varied during the run to expand the range of applicability.[26,34] This *programmed field* technique is not utilized here because the results obtained under variable crossflow conditions are more difficult to interpret in relationship to fundamental parameters. Other alternate forms of FFF operation include the use of asymmetrical channels[26-28,35-37] and hollow fibers,[38] which are subject to somewhat different (and more complicated) theoretical treatments.

Resolution and Plate Height. As noted above, separation requires that a difference Δt_r in retention time t_r be generated by the unequal hydrodynamic diameters or diffusion coefficients of the components subjected to fractionation. However, separation also requires that peak broadening be contained so that peaks with a finite Δt_r do not overlap. In FFF, theoretical guidelines can be developed to reach band broadening and resolution objectives by adjustments in the two flow rates $\dot{V}$ and $\dot{V}_c$.

As in chromatography and related techniques, the resolution R_s between two components can be defined by[20]

$$R_s = \frac{t_{r2} - t_{r1}}{2\tau_2 + 2\tau_1} \cong \frac{\Delta t_r}{4\tau} \tag{12}$$

where τ_2 and τ_1 are the standard deviations (in time units) of the two eluting peaks. For flow FFF the τ values tend to be relatively constant from one component to the next[30] and are represented simply by τ. In elution methods such as FFF and chromatography, τ is related to the plate height H by[20]

$$H = L\tau^2/t_r^2 \tag{13}$$

The combination of eqs 12 and 13 gives

$$R_s = \frac{L^{1/2}}{4}\frac{\Delta t_r}{t_r H^{1/2}} \tag{14}$$

The nonequilibrium contribution to the plate height in flow FFF, which is the irreducible minimum value of H, is closely approximated by[30]

$$H = \frac{2}{3}R^2(1-R)\frac{\dot{V}}{\dot{V}_c}L \cong \frac{2}{3}R^2\frac{\dot{V}}{\dot{V}_c}L \tag{15}$$

where the final approximation is applicable for R (or λ) $\ll 1$. When this latter approximation is substituted into eq 14, we get

$$R_s = \frac{1}{4}\left(\frac{3}{2}\frac{\dot{V}_c}{\dot{V}}\right)^{1/2}\frac{\Delta t_r}{t_r R} \tag{16}$$

The first part of eq 1 shows that the product $t_r R$ is a constant equal to t^0. Using this and employing eq 7 to get Δt_r, we arrive at the resolution expression

$$R_s = \frac{\pi}{8}\left(\frac{3}{2}\frac{\dot{V}_c^3}{\dot{V}}\right)^{1/2}\frac{\eta w^2}{kTV^0}\Delta d \tag{17}$$

where Δd is the difference in hydrodynamic diameters between the two species being separated. Equation 17 shows that resolution can be enhanced by increasing the crossflow rate $\dot{V}_c$ or decreasing the channel flow rate $\dot{V}$. However, the resulting gain in resolution comes at the expense of longer run times. This is confirmed by eq 8 which shows that t_r has a similar dependence upon $\dot{V}_c$ and $\dot{V}$ as does R_s.

Diffusion Equations for DNA

Since flow FFF is capable of measuring the translational diffusion coefficient D, the friction coefficient f, and the hydrodynamic diameter d of DNA in solution as shown by eqs 8–11 and the more rigorous eq 1, values of these transport parameters can be readily obtained by flow FFF. These measurements can be compared to the predictions of transport equations. Below we give equations representing four different theoretical and semiempirical treatments of linear DNA diffusivity and one for circular DNA. We also present a simple empirical equation for DNA diffusion coefficients. The theoretical treatment of DNA diffusion is complicated by the high charge and the relatively high stiffness of the double helix chains, which exhibit a persistence length of ~50 nm (147 base pairs, 97 000 Da) at an ionic strength of 0.1 M.[39-41] Until molar masses reach well into the millions, where flexible-chain theory can be used, DNA diffusion is complicated by wormlike behavior.[42,43] Some of the treatments described below allow for rodlike and wormlike behavior, and others apply only to the high-M limit of random coils.

We note that the mean-square radius of gyration for a wormlike chain is provided to a reasonable approximation by the Kratky–Porod theory[44]

$$\langle R_g^2 \rangle = 2p\mathcal{L}\left[\frac{1}{6} - \frac{p}{2\mathcal{L}} + \frac{p^2}{\mathcal{L}^2} - \frac{p^3}{\mathcal{L}^3}(1 - e^{\mathcal{L}/p})\right] \tag{18}$$

where p is the persistence length and $\mathcal{L}$ is the contour length of the DNA chain. For very long chains $\langle R_g^2 \rangle$ approaches $p\mathcal{L}/3$; it also approaches one-sixth the mean-square end-to-end length of the chain, which is a general property of random-coil polymers.[45]

Kirkwood–Riseman Approximation. The Kirkwood–Riseman equation for the friction coefficient of a flexible

nondraining chain based on the bead–spring model is[46]

$$f = \frac{n\zeta}{1 + (8/3)\lambda_0 n^{1/2}} \tag{19}$$

where n is the number of beads in the chain, ζ is the friction coefficient of a single bead, and λ_0 is given by $(6/\pi)^{1/2}a/b_0$ in which a is the bead radius and b_0 is the distance between adjacent bead centers. A further treatment by Flory provides a relationship between hydrodynamic radius $d/2$ and the root-mean-square radius of gyration R_g (assuming $\langle R_g^2 \rangle = b_0^2 n/6$).[45]

$$d/2 = 0.665R_g \tag{20}$$

The D based on the substitution of this $d/2$ into the Stokes–Einstein equation is

$$D = \frac{kT}{6\pi\eta(0.665R_g)} \tag{21}$$

This expression, with R_g obtained from eq 18 (using p = 50 nm), has been used to generate a diffusion coefficient plot to be shown later (Figures 11 and 12) in comparison with experimental data. We note that although the wormlike chain model used to obtain eq 18 is quite unlike the bead–spring model leading to eq 20, the above combination of approaches has been reported several times in the literature.[47-49]

Mandelkern–Flory Approach. For a random-coil polymer the friction coefficient can be approximated by[50]

$$f = \eta P \Phi^{-1/3}(M[\eta])^{1/3} \tag{22}$$

where P = 5.1, $\Phi = 2.1 \times 10^{23}$, and $[\eta]$ is the intrinsic viscosity of the polymer. There are several empirical equations for the $[\eta]$ of DNA that yield similar results.[51-53] We use the expression of Crother and Zimm (applicable to the M range $\sim 3 \times 10^5$ to 10^8 Da).[51]

$$[\eta] = 1.3709 \times 10^{-3} M^{0.665} - 5.0 \tag{23}$$

When this expression and the numerical values given above for P and Φ are substituted into eq 22 and thereafter into the Einstein equation, the diffusion coefficient becomes

$$D = \frac{(1.1655 \times 10^7)kT}{\eta(1.3709 \times 10^{-3} M^{1.665} - 5.0M)^{1/3}} \tag{24}$$

Tirado–Garcia de la Torre Theory. This theory applies in the low-M range where DNA can be treated as a rigid rod. In this case D is[54]

$$D = \frac{kT}{3\pi\eta\mathcal{L}}\left[\ln\left(\frac{\mathcal{L}}{\delta}\right) + 0.312 + 0.565\left(\frac{\delta}{\mathcal{L}}\right) - 0.1\left(\frac{\delta}{\mathcal{L}}\right)^2\right] \tag{25}$$

where the parameters were defined earlier. Our calculation use δ = 2.5 nm.

Yamakawa–Fujii Theory. This theory utilizes the wormlike cylinder model (without excluded-volume effects) to evaluate D.[55] The Oseen–Burgers procedure was used to account for hydrodynamic interactions. The distribution function and friction coefficient were obtained using the second Daniels' approximation[56] and the cubic approximation of Hearst and Stockmayer.[57] Their equation is

$$D = skT/3\pi\eta\mathcal{L} \tag{26}$$

where the dimensionless parameter s is a complicated function of $\mathcal{L}$, p, and δ. Our calculations based on eq 26 are made using p = 50 nm and δ = 2.5 nm.

Fujii–Yamakawa Theory of Circular Chains. The Yamakawa–Fujii theory of wormlike chains cited above was extended to wormlike rings.[58] The theoretical D can be expressed in the same form as eq 26 with s assuming a different dependence on chain parameters to account for ring behavior.

Experimental Section

Flow FFF. The details of the flow FFF system were described in a previous paper.[59] The flow FFF channel has approximately the same geometry and is constructed of the same material as that utilized in the Model F-1000 flow FFF system from FFFractionation, Inc. (Salt Lake City, UT). This channel has a volume-based length $L = V^0/bw$ = 30.0 cm. The channel breadth b is 2.1 cm, and the thickness w is 254 μm. The geometric (calculated from dimensions) void volume is 1.60 mL, whereas the V^0 measured by the breakthrough procedure[60] was 1.43 mL, giving an experimental channel thickness of 227 μm. (The latter two values varied a few percent each time the channel was reassembled after cleaning, but the newly measured values were used in all calculations.) The experimental and nominal dimensions differ because of the compression of the membrane used at the accumulation wall.[60] This membrane is a Diaflo ultrafiltration YM-30 membrane from Amicon (Amicon Division, W. R. Grace Co., Beverly, MA). Outlet flow constrictors consisting of lengths of 250-μm-i.d. capillary tubing were used to control both channel flow and crossflow rates. The flow rates were measured by a buret and a stopwatch. The sample injection valve, Model 7010, was from Rheodyne (Cotati, CA). The sample loop volume was 35 μL and had a relatively large (787 μm) inside diameter to prevent shear degradation. The DNA samples were injected into the loop by a single-use 1-mL syringe (Becton Dickson & Co., Rutherford, NJ) without a needle. The sample was carried into the channel by a 0.091-mL flow displacement, after which the flow was stopped for an interval (the stopflow time t_{sf}) for relaxation in the ongoing crossflow. A Model 757 UV detector from Applied Biosystems (Ramsey, NJ) was used for detection at 260-nm wavelength. The signal was registered by an Esterline Angus (Indianapolis, IN) SS 250F recorder. The pump used for the channel flow was a Kontron Model 414 LC pump (Kontron Electrolab, London, U.K.). The flow source for crossflow was a type CMP Cheminert metering pump (Chromatronics, Berkeley, CA). All experiments were run at laboratory temperatures (23 ± 1 °C) with acquired diffusion coefficients corrected to water at 20 °C using a viscosity correction factor of 0.964.

Chemicals and Samples. Doubly-distilled water, boiled for 10 min before preparing the carrier solution to avoid contamination by DNase, was used throughout. The carrier solution was a Tris-HNO_3 buffer of ionic strength 0.1 M and with pH 8.0 at 25 °C with 1.0 mM EDTA. The Tris base was obtained from Sigma Chemical Co. (St. Louis, MO) and the EDTA from Fisher Scientific (Fair Lawn, NJ).

DNA Samples. The plasmid pBR322 was purchased both from Bethesda Research Laboratory (Gaithersburg, MD) and Boehringer Mannheim Biochemicals (Indianapolis, IN). The latter was also the source of M13mp18 RF I, pUC18, and M13mp9 (a single strand). The restriction enzymes, φX174 RF I and φX174 virion (a single strand), came from New England Biolaboratories (Beverly, MA). The concentration of the injected DNA varied from 1.0 to 5.0 μg/100 μL (10–50 ppm). DNA digestion and recovery were carried out according to Maniatis et al.[61]

Plasmids and viral circular DNAs were cut at specific sites by enzymes to produce the linear DNA fragments studied here. The experimental steps are shown in Figure 2. Table I lists all of the linear DNA fragments used in this study. The sizes range from 657 to 4961 bp with Ms from 4.3×10^5 to 3.3×10^6 Da.

Separation of DNA

Separation of Single- from Double-Stranded Circular DNA. Because of the greater flexibility of single DNA strands ($p \sim 18$ nm[62]), they fold into more compact structures than double strands ($p \sim 50$ nm) of equivalent contour length. The resulting difference in size, friction coefficient, and diffusion coefficient makes single and double strands separable by flow FFF. (As noted earlier, single and double strands can also be separated by

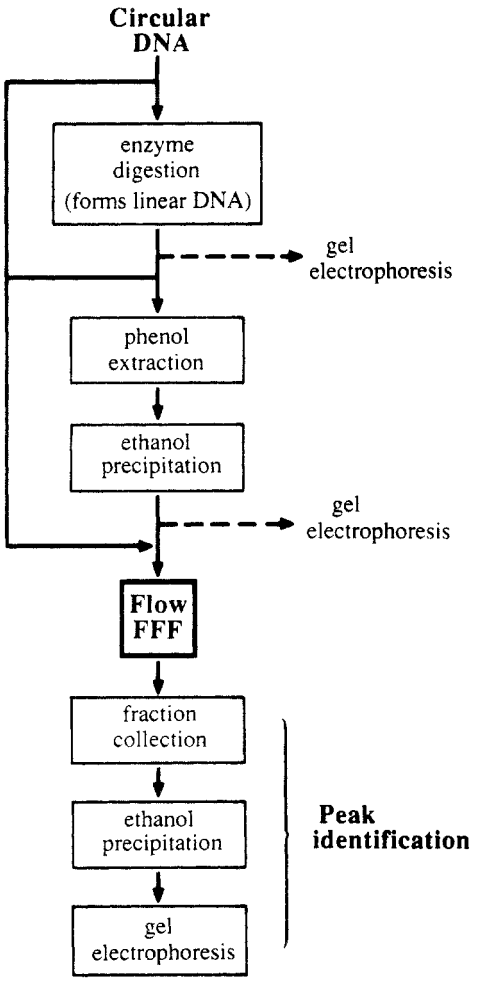

Figure 2. Experimental scheme for the preparation and utilization of DNA molecules.

Table I. Linear DNA Fragments from Enzyme Digestion Used for Flow FFF Studies

DNA	enzyme	linear fragments M^a	linear fragments bp[b]
M13mp18 RF I	*Xmn*I	3 274 260	4961
		1 510 740	2289
	*Nde*I	2 063 820	3127
		2 008 380	3043
		712 800	1080
pBR322	*Eco*RV	2 878 260	4361
	*Dra*I	2 409 000	3650
		456 720	692
	*Nar*I	2 355 540	3569
		433 620	657
	*Hinc*II	2 147 640	3254
		730 620	1107
pUC18	*Sca*I	1 772 760	2686
	*Dra*I	1 303 500	1975
		456 720	692

[a] M = molecular weight in Da. [b] bp = base pairs.

sedimentation FFF but in this case the separation is based on the different masses of the two DNAs.) This separability is illustrated by Figure 3b, with the single-stranded DNA M13mp9 (7599 b) separated cleanly from the double-stranded analog M13mp18 RF I (7250 bp). The separation is completed in about 22 min, but because the resolution is higher than required, the excess resolution could be traded for increased speed. This strategy will be demonstrated later.

In order to verify that the two successive peaks correspond to the single and double strands, respectively, these can be injected individually to verify the match of their

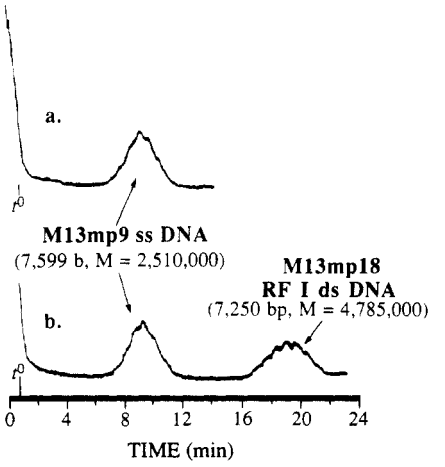

Figure 3. Separation of single- and double-stranded circular DNAs by flow FFF. The number of bases (b), base pairs (bp), and molecular weights (M) are shown. Experimental conditions are $\dot{V}$ = 3.16 mL/min, $\dot{V}_c$ = 1.04 mL/min, and t_{sf} = 2.0 min. Amount injected = 0.194 μg each.

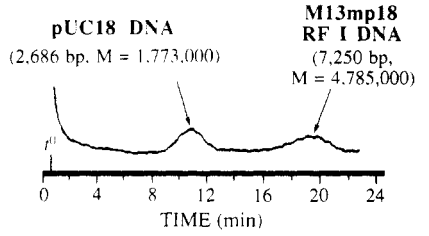

Figure 4. Separation of two double-stranded circular DNAs of different sizes (as indicated in the figure) by flow FFF. Conditions are $\dot{V}$ = 3.13 mL/min, $\dot{V}_c$ = 1.08 mL/min, and t_{sf} = 2.0 min. Amount injected = 0.091 μg each.

retention time with that of the peaks. Thus in Figure 3a the single-stranded DNA is run alone and shown to produce a single peak equivalent to the first peak produced from the mixture (Figure 3b). Since t_r is roughly proportional to d (see eqs 5 and 6), the relative peak positions reflect the smaller size of the single-stranded circular DNA. The use of such retention data to produce experimental values of d, D, and f will be described below.

Separation of Circular DNAs. Double-stranded circular DNAs of different size can similarly be separated by flow FFF by virtue of differences in D or d. This is illustrated in Figure 4 which shows the separation of plasmid pUC18 and M13mp18 RF I DNA. These two DNAs differ by a factor of 2.70 in M (7250 versus 2686 bp); the ratio of t_rs and thus the ratio of d values is shown by Figure 4 to be 1.85. As in Figure 3, the resolution is beyond that needed for purification.

Separation of Linear DNA Fragments. The linear double-stranded fragments listed in Table I have been subjected to flow FFF analysis both to obtain diffusion coefficients and to examine the separability of linear chains. Figure 5 shows the separation of 1107 and 3254 bp fragments at two different channel flow rates. In Figure 5a the resolution exceeds that required for purification, suggesting, in accordance with the discussion of eq 17, that the excess resolution can be traded for speed. This tradeoff is most easily achieved by increasing the channel flow rate $\dot{V}$. Thus holding $\dot{V}_c$ constant at 1.05 mL/min, $\dot{V}$ is changed from 3.15 mL/min in run a to 6.7 mL/min in run b. This 2.1-fold increase in $\dot{V}$ leads to a 2.1-fold decrease in the run time (from 20 to just under 10 min) as predicted by eq 8. According to eq 17, the resolution loss from run a to run b should be from R_s = 3.61 to R_s = 2.48, a factor of 1.46. The experimentally measured R_s

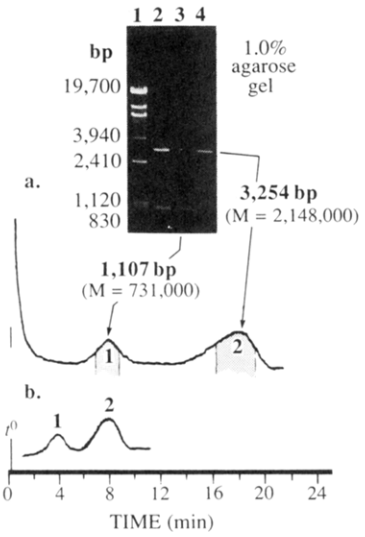

Figure 5. Separation of linear DNA fragments of 1107 and 3254 bp. The tradeoff of speed for excess resolution is attained by increasing $\dot{V}$ from 3.15 to 6.7 mL/min with $\dot{V}_c$ held at 1.05 mL/min in both cases. The identity and integrity of the fragments collected from the eluting stream are confirmed by electrophoresis as shown. The sample was obtained by the *Hinc*II digestion of 0.35 μg of pBR322.

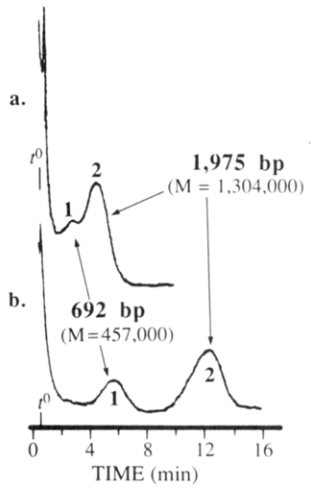

Figure 6. Separation of 692 and 1975 bp linear DNA fragments by flow FFF. The increase in resolution at the expense of speed in going from fractogram a to b is generated by increasing $\dot{V}_c$ from 0.42 to 1.05 mL/min. The sample was obtained by the *Dra*I digestion of 0.33 μg of pUC18.

in the two cases is 2.2 and 1.53, values somewhat lower than those predicted. The ratio of the observed resolutions is 1.4–1.5, comparable to the 1.46-fold resolution loss predicted.

The identification of the two peaks in Figure 5 with corresponding DNA fragments is well assured by the fact that t_r is proportional to d (eq 8), requiring that the second peak contain the larger (3254 bp) fragment. For further proof, fractions were collected and subjected to gel electrophoresis. The results, also presented in Figure 5, confirm the expected peak identities and the lack of DNA degradation during the run.

We find that the relative area of peak 2 to peak 1 in Figure 5 is 2.9. This ratio is verified in our subsequent overloading work (Figure 9); altogether seven measurements yield the ratio 2.89 ± 0.03. The 2.9/1 ratio corresponds closely to the expected contents of the two peaks, which should follow the base-pair ratio 3254/1107 = 2.94. This suggests that flow FFF yields a proportionate recovery of different-sized DNA fragments. The absolute recovery of DNA is also quite high as verified by the fact that the electrophoretic bands of DNA recovered between the cut positions shown for fractogram a of Figure 5 are 70 and 85% (for 1107 and 3254 bp, respectively) as wide as those from the original sample even though the DNA fractions from flow FFF do not incorporate the entire DNA peak content and they require several additional steps including fraction collection, ethanol precipitation, and resuspension. However, 85% of the original band width does not represent 85% absolute recovery because the relationship is not linear.[20]

A quite different example of resolution and speed manipulation is shown in Figure 6, which involves smaller DNA fragments of 692 and 1975 bp, respectively. For both runs $\dot{V}$ = 3.15 mL/min. However, when $\dot{V}_c$ = 0.42 mL/min (fractogram *a*), the first peak is not very well retained (t_r does not much exceed t^0) and the resolution, as typical in such cases, is poor. For such poorly retained peaks, the resolution is best augmented by increasing $\dot{V}_c$ although this will lead to a proportionate increase in the run time as shown by eq 8. A second run (fractogram b) with $\dot{V}_c$ increased to 1.05 mL/min confirms the predicted trends, with the run time increasing ~2.5-fold (in proportion to $\dot{V}_c$) and the resolution increasing to 1.8. This resolution compares reasonably well with R_s = 2.49 predicted from eq 17 with the two d values obtained from eq 8.

As described above, the fractograms in Figures 5 and 6 display a resolution inferior to that predicted by eq 17. This discrepancy is caused by imperfections in the system leading to peak broadening in excess of the theoretical minimum. Such discrepancies, common in flow FFF, have been largely eliminated in sedimentation FFF.[63] The elimination of this discrepancy by ongoing work in flow FFF will further enhance the resolution and speed of flow FFF separation.

Preparative Capacity. Purified components can be readily collected as they elute from an FFF channel using a fraction collector. It is important to determine the amount of material that can be separated in a single run. The preparative capacity of the system is then the amount separated per run multiplied by the number of runs employed. The number of runs can be large because FFF systems can be readily automated.

It is well known that, as sample amounts are increased, the eluting peaks shift in position, broaden, and become distorted relative to the ideal Gaussian elution profile.[64,65] These changes in peak shape and position, which ultimately lead to peak overlap and a loss of purity, result mainly from various types of interactions (both attractive and repulsive) between individual macromolecules. For long-chain polymers such "overloading" effects increase with M because of increasing chain entanglement. Factors affecting the overloading of random-coil polymers have been discussed in the literature.[64]

For the runs shown in Figures 3–6 the single-component quantities injected ranged from 0.085 to 0.261 μg. These quantities are ideal for analytical purposes, large enough to be readily detectable but small enough to avoid overloading effects such as shifts in retention times that would perturb the measurement of diffusion coefficients and compromise peak identification. Below we examine the consequences of increasing the sample load in pursuit of preparative objectives.

Figure 7 shows the fractograms obtained by injecting equal amounts of the two circular DNAs, single-stranded φX174 virion and double-stranded φX174 RF I. The amount varies between runs as shown in the figure from

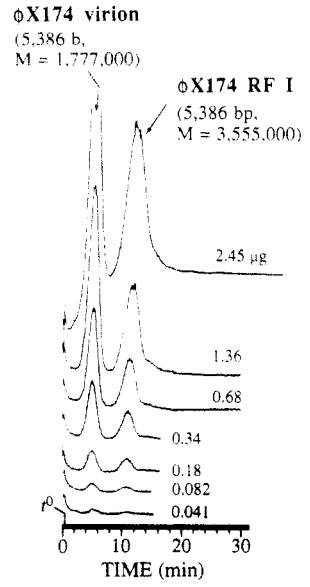

Figure 7. Effect of sample load on the resolution of single-stranded and double-stranded circular DNAs. The amount (in micrograms) of each component injected is shown in the figure. Conditions are $\dot{V}$ = 3.16 mL/min, $\dot{V}_c$ = 0.86 mL/min, and t_{sf} = 2.3 min.

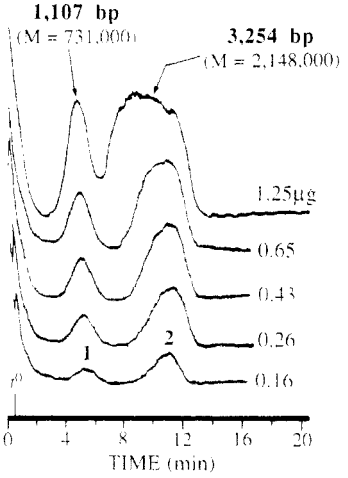

Figure 8. Effect of sample load on the resolution of linear DNA chains. The injected amounts shown are those for the longer DNA fragment (second peak); the first peak has an equal number of molecules but 2.94 times less mass for each injection. Run conditions are $\dot{V}$ = 3.25 mL/min, $\dot{V}_c$ = 0.84 mL/min, and t_{sf} = 2.0 min.

0.041 to 2.45 μg. The figure shows a gradual broadening of the double-stranded DNA peak over this range. However, because we start with an excess of resolution, the resolution remains satisfactory over this sample load range despite the gradual increase in peak breadth.

A similar outcome is found by increasing the sample load of linear DNA chains as shown in Figure 8. These results, obtained for 1107 and 3254 bp DNA, again show a significant broadening of the high-M peak as the load increases. The effect appears to be more severe with the linear than the circular chains despite their similar hydrodynamic diameters.

The more rapid broadening of the second peak compared to the first peak in both Figures 7 and 8 is the result of the higher compression (and thus concentration) of the higher M material against the accumulation wall of the channel. This broadening is augmented by the longer chain length of DNA in the second peak and the increased tendency for chain interaction and entanglement. In addition, for Figure 8 the injected mass of the larger DNA is 2.94 times higher than that of the shorter chain DNA. It is interesting that in both Figures 7 and 8 (but more so in Figure 8) the second peak shifts toward lower retention times as the sample load increases. This behavior is more typical of charge-bearing colloidal particles[65] than of neutral polymers[64] and probably originates in the mutual repulsion of the negatively charged DNA molecules.

High Molecular Weight DNA. As one proceeds to longer DNA chains ($M > 10^7$ Da), the behavior of DNA in FFF systems significantly changes. First, increasing chain entanglement amplifies overloading, requiring reduced sample loads and increased detector sensitivity. Longer DNA chains are also more susceptible to shear degradation. Additionally, the increasing physical size of the DNA coil brings a new mechanism of FFF (the steric mechanism) into play. The steric mechanism at first perturbs the retention described in our theoretical treatment but eventually controls retention, alters its theoretical basis, and leads to an inversion of elution order (long chains preceding short chains). Finally, the shear-induced elongation of polymers appears to lead to additional transverse forces (called lift forces) that further perturb retention and contribute to the retention inversion noted above.

In principle, these changes should not interfere with the successful separation of DNA. As long as the transverse forces (including lift forces) are sensitive to M and remain strong enough to drive DNA chains of different lengths into different localized stream laminae, and as long as dilutions are high enough to avert chain interactions, the differential migration and separation of DNA bands should be observed. We must also assume that the relaxation time for conformational changes is a small fraction (preferably $<10^{-3}$) of the elution time since different conformations of a given DNA chain will have different properties.

In an attempt to adapt to the above changes, we have used three different flow FFF channels. Channel I was constructed with a split inlet, which reduces shear during sample introduction and bypasses the need for stopflow relaxation.[66] Channel II was made with both a frit inlet and a frit outlet.[66] The frit inlet provides the same advantages as the split inlet but can be used with thinner channels (in this case 254 versus 330 μm nominal thickness). The frit inlet was further modified by drilling a hole through the upper frit to introduce sample beyond the channel tip where the shear stress is greatest. The frit outlet of channel II permits enrichment of the sample (up to 16-fold) at the outlet to improve detectability. Channel III is a conventional flow FFF channel as described earlier. Gel electrophoresis (0.4% agarose) was used to examine shear degradation. The samples examined in this study included T2, T7, λ, and Micrococcus leteus DNAs with Ms of 110, 26.4, 32.0, and 64.0 × 10^6 Da, respectively.

The above efforts to separate high-M DNA were thwarted by overloading. At the highest detector sensitivity, even when amplified by the 16/1 enrichment of the frit outlet, the elution time of the DNA peaks depended strongly upon sample load, a classical symptom of overloading.[64] The peaks were very broad, a result consistent with overloading but not likely attributable to normal conformational changes since the relaxation time even for T2 DNA is only ~0.5 s.[67,68]

The susceptibility of long DNA chains to shear degradation has been recognized since 1959.[69] Shear degradation in channel I was studied using electrophoresis and less direct FFF evidence. The shear degradation of T2 DNA was observed over the flow rate range $\dot{V}$ = 0.2–6.9

mL/min, but T7 is degraded only at the upper extreme of this range. The observation[70] that T2 DNA remains intact at a shear rate of $s_0 = 5\ s^{-1}$ implies that channel I could be operated at 0.2 mL/min where $s_0 = 5.3\ s^{-1}$. The observation of degradation at this flow rate is probably attributable to high s_0 values ($\sim 10^2\ s^{-1}$) in the delivery tubing and at the channel tips. (Extensional shear also occurs in the tip regions.) These problems could be rectified by using larger tubing and channels that are thicker near the tip. Also the DNA can be introduced well back from the tip as described for channel II. Thus, while the shear degradation problem is likely solvable for $M \sim 10^8$ Da, the $1/M^2$ dependence of the "critical" shear rate[71,72] may limit further gains in the applicable M range.

As noted above, steric effects become significant when the physical dimensions of the DNA coil become a significant fraction of the Brownian displacement distance λw. Retention (as described by eq 6) must then be modified by the addition of a steric term[73]

$$R = 6\lambda + 3\gamma d_{st}/w \tag{27}$$

where γ is the steric correction factor ($\gamma \approx 1$) and d_{st} is the *steric diameter* of the coil, which can be taken as the maximum extension of the polymer chain along the crossflow axis. By combining eqs 6 and 7 and $V^0 = bLw$, eq 27 becomes

$$R = \frac{2kTV^0}{\pi\eta\dot{V}_c w^2 d} + 3\gamma\frac{d_{st}}{w} \tag{28}$$

For a random-coil polymer d_{st} can be obtained from[74]

$$d_{st}/2 = 1.69R_g \tag{29}$$

which is analogous to eq 20. Since R_g can be assumed proportional to $M^{0.6}$, eqs 20 and 29 give $d = B_h M^{0.6}$ and $d_{st} = B_{st}M^{0.6}$, where B_h and B_{st} are constants. Thus eq 28 becomes

$$R = \frac{2kTV^0}{\pi\eta w^2\dot{V}_c B_h M^{0.6}} + 3\gamma\frac{B_{st}M^{0.6}}{w} = \frac{\alpha_1}{M^{0.6}} + \alpha_2 M^{0.6} \tag{30}$$

At sufficiently large M the second term on the right dominates, giving steric FFF. This form of FFF has been widely used for rigid particles over $\sim$1-μm diameter[73,75] but not for polymers. For steric FFF, R increases with M whereas R normally decreases with M in accordance with the first term on the right-hand side. The transition (or inversion) point occurs at $M = M_i$ for which $dR/dM = 0$. Differentiation gives

$$M_i = \left(\frac{\alpha_1}{\alpha_2}\right)^{5/6} = \left[\frac{2KT(V^0/\dot{V}_c)}{3\pi\eta w\gamma B_h B_{st}}\right]^{5/6} \tag{31}$$

If we assume $V^0/\dot{V}_c = 600$ s, $T = 293$ K, $\eta = 10^{-2}$ P, $w = 254\ \mu$m, and $\gamma = 1$ and if B_h and B_{st} are taken as 3.37 and 8.56×10^{-9} cm/Da$^{0.6}$ (based on eqs 20 and 29) and a literature expression for R_g,[76] we get $M_i = 23.6 \times 10^6$ Da. While overloading for $M \sim M_i$ has made it impossible to observe the transition phenomenon, higher detector sensitivity should make this transition observable.

We note that evidence exists for the generation of substantial shear-based lift forces on high M polymers at high shear rates ($\sim 10^3\ s^{-1}$) in FFF channels.[77] These forces would effectively increase γ in the foregoing equations. However, the phenomenon requires more documentation before its effects can be evaluated.

Since the application of FFF to high-M DNA is hindered by chain entanglements and eventually by shear degradation, another potential approach is to condense DNA into small compact particles prior to separation. This approach is attractive not only for avoiding entanglement (thus greatly increasing sample capacity) and degradation problems but also because FFF has proven highly effective in the separation of colloidal particles. Using sedimentation FFF, particles differing in diameter by only 10% (and thus in mass by about 30%) are resolvable.[78] In one case a mass difference of 10% has been resolved.[79]

The condensation of DNA, first demonstrated by Lerman in 1971,[80] is promoted by various salts (especially those with multivalent cations) and by water-soluble polymers such as poly(ethylene oxide) (PEO). The mechanism of condensation, the shape of the particles (which may not be spherical), and the formation of aggregates have been discussed by a number of authors.[81-84] Sizes may range from 35 to 125 nm.

Two condensed DNAs were prepared starting with 1.25–6.25 μg/mL of T2 or T7 DNA in a 50 mM sodium phosphate buffer (pH = 7.0) with 0.6 M NaCl, 1 mM EDTA, and 100 mg/mL of M = 8000 Da PEO. Electron microscopy showed both ellipsoidal particles and aggregates. The T2 particles were about 100 nm, as in the literature.[84] Unfortunately, the concentrations were too low to yield a detectable signal in most cases. Using the highest T2 DNA concentration (6.25 μg/mL), a broad peak emerged with $d \sim 163$ nm. The broad peak and the large d may be attributed to aggregation, which naturally accompanies condensation at higher DNA concentrations. However, aggregates should be separable by FFF. More work is needed to clarify this anomaly and to implement separation.

While none of the above approaches led to the successful separation of high-M DNA, we believe that our results and conclusions establish a basis for further progress in this field. Below we offer a brief summary of our conclusions.

First, combining the fact that ultralong DNA chains are sensitive to shear with the fact that FFF is based on a flow-shear mechanism suggests that FFF will be difficult to apply to random coils over about 10^8 molecular weight. (This constraint applies to all flow systems; it is more restrictive for chromatography than FFF because of extensional shear in column packing.) However, DNA condensation may provide a means for applying FFF to DNA with $M > 10^8$ Da. Lacking condensation, the FFF mechanism is expected to undergo a transition to steric or hyperlayer FFF at $M > 10^7$ Da. While these mechanisms are poorly understood for random coils, the inherent physical nature of FFF makes these mechanisms promising for separation. As long as transverse forces acting to drive DNA into localized stream laminae are strongly dependent upon M, the final positions within the stream laminae, and thus the velocity of displacement and the resulting elution time, should be quite sensitive to M as well. Thus if the concentration of DNA can be reduced by using a more sensitive detector, the effective separation of long DNA chains by FFF is a reasonable prospect. This possibility merits further study.

Measurement and Correlation of DNA Diffusivity

The basis for obtaining the translational diffusion coefficient D for DNA in solution by the measurement of retention times and the use of eq 11 (or a somewhat more exact form based on eq 1) was described above. Based on this treatment, Ds were measured for all DNA molecules employed in this study, both circular and linear. For tabulation, these D values have been viscosity-corrected to pure water at 20 °C. (Such a correction does not account for electrostatic-based chain expansion in the absence of

Table II. Translational Diffusion Coefficients and Hydrodynamic Diameters of DNA Measured by Flow FFF

DNA	mol wt (Da)	$D_{20,w} \times 10^8$ (cm²/s)	d (nm)
	Circular DNA		
M13mp9 (ss)[a]	2 507 670	5.01	87
ϕX174 virion (ss)	1 776 380	6.76	64
M13mp18 RF I (ds)[b]	4 785 000	2.44	178
ϕX174 RF I (ds)	3 554 760	3.22	135
pUC18 (ds)	1 772 760	4.43	98
	Linear DNA		
1	3 274 260	2.30 ± 0.09[c]	189
2	2 878 260	2.37 ± 0.12	183
3	2 409 000	2.54 ± 0.20	171
4	2 355 540	2.92 ± 0.13	149
5	2 147 640	3.04 ± 0.18	143
6	2 036 477	3.11 ± 0.10	139
7	1 772 760	3.43 ± 0.10	126
8	1 510 740	3.77 ± 0.11	115
9	1 303 500	4.06 ± 0.17	107
10	730 620	6.50 ± 0.13	67
11	712 800	6.47 ± 0.15	67
12	456 720	8.98 ± 0.31	48
13	433 620	9.42 ± 0.41	46

[a] ss = single-stranded DNA. [b] ds = double-stranded DNA. [c] Standard deviation based on 3–7 measurements.

electrolyte; rather the chain conformation is assumed unchanged by transfer to 20 °C water.)

Our measurements are summarized in Table II. With each tabulated D value we show the corresponding hydrodynamic diameter d calculated from the Stokes–Einstein equation. Unfortunately, a paucity of literature data makes the direct comparison of Ds obtained by flow FFF and other methods difficult. (An exception is pUC8 (2717 bp) for which $D = 4.90 \times 10^{-8}$ cm²/s has been reported.[85]) However, Table II shows reasonable precision in the D values from flow FFF; the average standard deviation is 4.1%.

Because diffusivity data are scarce for individual DNAs, the correlation of D with chain length (or molecular weight) using a combination of flow FFF data, literature data, and appropriate equations appears to be the best approach for converging upon meaningful diffusion coefficients for specific DNAs lacking experimental data. Further D measurements will, of course, help refine the correlation. (A strict correlation between D and chain length will of course not exist for double-stranded circular DNA with a variable number of superhelical turns.) Once a good correlation is established, flow FFF retention measurements can be converted directly to molecular weight values, thus helping identify isolated DNA peaks.

While no rigorous theory is available to calculate the diffusivities of circular DNAs, estimates can be obtained from the theory of Fujii and Yamakawa.[58] Figure 9 shows plots of D versus M (using Logarithmic scales) for circular DNAs based on the Fujii–Yamakawa treatment. The chain diameters for single and double strands are assumed to be 1.3 and 2.5 nm, respectively. Plots are made for a persistence length of $p = 50$ nm for double strands and different assumed persistence lengths for single strands. Experimental data, both from flow FFF (Table II) and from the literature[47,49,62,85–97] (Table III), are shown for comparison. Consistent trends are found except for the literature values (solid circles) for single strands, which are unduly scattered. The correlation between theory and experiment (open squares and circles) is observed to be quite good for double strands. The limited FFF data (two solid squares) for single strands agree best with the plot based on $p = 25$ nm. By comparison, a recent p value from the literature is 18 nm.[62]

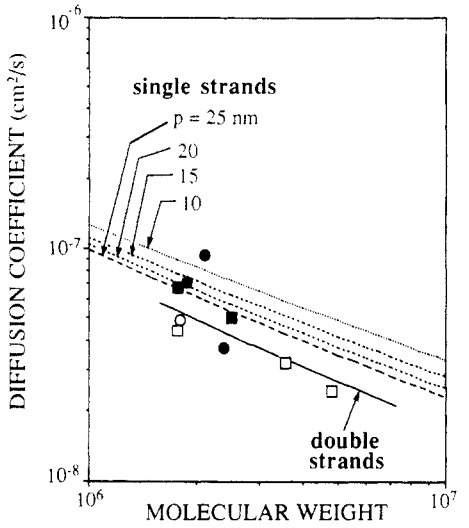

Figure 9. Diffusion coefficient plots for single- and double-stranded circular DNA. The upper four plots are from Fujii–Yamakawa theory based on different persistence lengths p ranging from 25 to 10 nm as shown. The plot at the bottom is based on Fujii–Yamakawa theory applied to double strands. Flow FFF data are shown by squares and literature values by circles. The solid symbols refer to single strands, and the open symbols pertain to double strands.

As outlined earlier, a more extensive theoretical framework is available for examining trends in the diffusivity of linear double-stranded DNA. Figure 10 shows the experimental D data from flow FFF alongside the plots generated from the four theoretical and semiempirical treatments described earlier. The data agree quite well (average deviation = 2.6%) with the Mandelkern–Flory expression (eq 24) but also fit reasonably well to the other plots which define a fairly narrow band (even with rigid-rod theory included) up to a few million molecular weight. Somewhat surprisingly, rigid-rod theory (described by the Terado–Garcia de la Torre plot from eq 25) appears to work well up to and beyond 10^6 Da molecular weight, equivalent to a contour length of about $10p$ (500 nm), whereas a rigid rod is not a realistic model of DNA beyond $\sim 0.3p$.[42]

A literature search was undertaken to expand the empirical base of D values and further clarify trends. A compilation of these diffusivities (and the method of acquisition) is provided in Table III.[47,49,62,85–97] Since data from the literature set apply to both longer and shorter chains than measured by flow FFF, a new plot covering an expanded range showing all of the experimental results (both from flow FFF and from other methods) in comparison to the theoretical expressions is shown in Figure 11. These plots extend down across the transition region from random-coil behavior to that of wormlike chains; the shortest pieces of DNA approach rigid rods. Unfortunately, the high-M data are quite widely scattered, making it difficult to examine trends for $M > 10^7$ Da. The Mandelkern–Flory expression (eq 24) provides a good fit to the experimental data down to $M = 4 \times 10^5$ Da but then diverges sharply upward. This divergence can be traced to eq 23 for intrinsic viscosity, for which $[\eta] \to 0$ at $M =$ 227 000 Da. An equation for $[\eta]$ applicable at low M might further extend the range of this approach. We note, as before, that rigid-rod theory provides a good fit up to an M of 2–3 million, corresponding to chains for which all vestiges of rodlike behavior have presumably disappeared. The Kirkwood–Riseman approach, by contrast, provides a D plot lying well beneath the bulk of the data set except at high M. The Yamakawa–Fujii theory provides a good

Table III. Literature Data

DNA	mol wt (Da)	$D_{20,w} \times 10^8$ (cm²/s)	d (nm)	method	ref
		Circular DNA			
fd (ss)[a]	1 870 000	7.07	61	DLS[c]	86
M13 (ss)	2 114 310	9.34	46	zonal diffusion	87
M13m19 (ss)	2 392 500	3.75	115	static LS	62
pUC8 (ds)[b]	1 793 220	4.90	88	DLS	85
		Linear DNA			
1	1 793 220	3.4	126	DLS	85
2	58 740 (89)	42.7	10	DLS	88
3	68 640 (104)	38.8	11	DLS	88
4	81 840 (124)	34.1	13	DLS	88
5	247 500 (375)	14	31	DLS	89
6	110 000 (150)	30	14	DLS	90
7	26.30 M	0.90	477	cell diffusion	91
8	14.10 M	1.1	390	cell diffusion	91
9	8.86 M	1.42	302	cell diffusion	91
10	6.88 M	1.69	254	cell diffusion	91
11	5.69 M	1.86	231	cell diffusion	91
12	1.95 M	3.61	119	cell diffusion	91
13	0.95 M	6.23	69	cell diffusion	91
14	1.5 M	5.1	84	DLS	92
15	12.0 M	1.67	257	DLS	92
16	4.37 M	2.12	203	DLS	93
17	4.30 M	1.98	217	DLS	94
18	1.53 M	4.42	97	DLS	95
19	666 600 (1010)	7.15	60	DLS	49
20	502 920 (762)	9.05	47	DLS	49
21	242 220 (367)	15.8	27	DLS	49
22	24.0 M	0.573	749	electron microscopy	96
23	38.3 M	0.342	1255	electron microscopy	96
24	4.30 M	1.95	220	DLS	47
25	31.60 M	0.649	662	DLS	97

[a] ss = single-stranded DNA. [b] ss = double-stranded DNA. [c] DLS = dynamic light scattering.

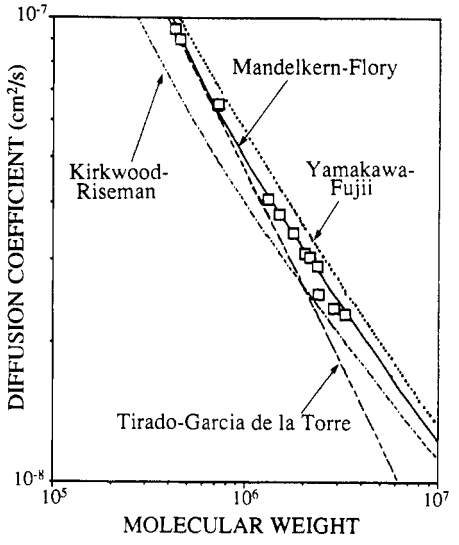

Figure 10. Diffusion coefficient plots for linear DNA from four theoretical treatments outlined in this paper in comparison to data from flow FFF measurements.

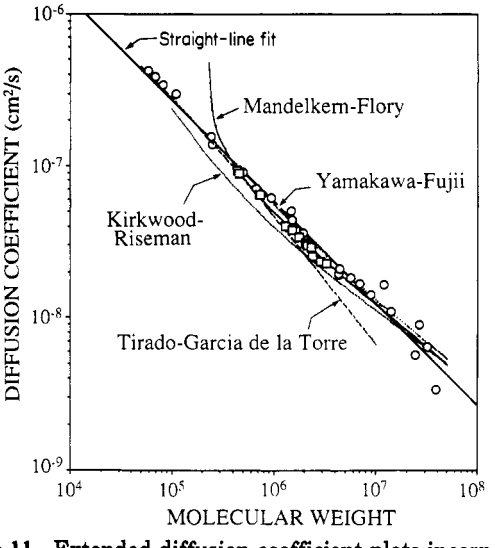

Figure 11. Extended diffusion coefficient plots incorporating both flow FFF data (squares) and literature values (circles).

fit of the data down to $M \cong 400\,000$ Da; a more complicated form of this theory applicable below $M = 200\,000$ Da has not been tested.

Interestingly, the experimental data plotted in Figure 11 show only a slight tendency to change slope as M increases. Consequently, we have investigated a linear representation of the log D versus log M data, or equivalently $D = AM^{-b}$. The straight line shown in Figure 11 shows that this type of plot provides a good fit of the data over the experimental range, which is almost 3 decades. The parameters found (using units of Da and cm²/s) are $A = 6.452 \times 10^{-4}$ and $b = 0.6762$. A fit to the FFF data alone yields $A = 9.603 \times 10^{-4}$ and $b = 0.7121$. The average deviation of the FFF data from its least-squares plot is 2.4%. (Circular DNA in the limited range of Figure 9 can also be described by eq 33 with b values, based in this case on the theoretical plots, equal to 0.66 for double strands and 0.62–0.58 for single strands with p decreasing from 25 to 10 nm, respectively.)

While the relationship $D = AM^{-b}$ is well established for random coils of large M,[42,45] it would not initially appear

likely to work for smaller M values where DNA chains are governed by wormlike and rodlike behavior. Thus for rigid rods, the slope of a log D versus log M plot is often assumed to be about −0.8,[42,98] a value inconsistent with the high-M limit of −0.55 to −0.60. However, the slope for rigid rods depends on the aspect ratio $m = \mathcal{L}/\delta$, as shown by the following expression obtained using eq 25:

$$\frac{d \log D}{d \log M} = \frac{\left(1 - \frac{0.565}{m} + \frac{0.2}{m^2}\right)}{\left(\ln m + 0.312 + \frac{0.565}{m} - \frac{0.1}{m^2}\right)} - 1 \cong \frac{1}{2.303 \log m} - 1 \quad (32)$$

The approximation on the right applies when $m \gg 1$. If we assume $\delta = 2.5$ nm and $M/\mathcal{L} = 1941$ Da/nm, then $m = 2.06 \times 10^{-4}$ M. A slope of −0.8 applies only at $m \cong 10^2$, for which $M = 485\,000$ Da and the chain is about 250 nm. However, this length exceeds the persistence length ($p \cong 50$ nm) by a factor of 5, and it exceeds the length of a DNA chain that can be considered rodlike by a factor of over 15. The latter is based on the Cantor and Schimmel[42] estimate that the contour length below which DNA is rodlike in solution is about $0.3p$, which is ~15 nm, a length for which the aspect ratio is only 6. At this critical length eq 33 gives a slope of only −0.415. While the slope changes rapidly to −0.646 for $m = 10$ and −0.709 for $m = 20$, such m values no longer correspond to rigid rods. Thus there is little justification for basing slope values on rigid-rod theory for data sets (such as ours) based on $M \geq 30\,000$ Da ($m \geq 6$).

Since limiting theories offer little guidance on the effectiveness of $D = AM^{-b}$ over a broad molecular weight range, we turn again to empirical evidence. While this equation agrees well with the experimental data, the least-squares b of 0.676 is clearly too large (by about 0.1) to describe long randomly coiled DNA molecules. Some of the fault may reside with the high-M data, which introduces the worst scatter. However, even with the three smallest D values eliminated from the data set, b is only reduced to 0.663. Thus it appears that the overall data set is influenced by factors leading to a larger b value than expected in the high-M limit. Therefore $D = AM^{-b}$, while a useful interim expression, is unlikely to provide high accuracy when judged against expanded and improved data sets (or more accurate theoretical expressions) resulting from future work. A nonconstant slope may better be taken care of by an expression of the form

$$D = \frac{A}{M^b} + \frac{B}{M^{0.6}} \quad (33)$$

where A, B, and b are adjustable parameters. As long as $b > 0.6$, this expression will approach the appropriate limit of an $M^{-0.6}$ dependency at high M. It is clearly important to acquire a larger quantity of better data to fully evaluate these possibilities.

Conclusions

It is clear from this and preceding studies that field-flow fractionation techniques are effective tools for the separation and characterization of DNA chains up to at least 10^7 Da. If overloading problems are bypassed, this capability will probably extend to much longer chains as well. The separation process itself is relatively rapid and simple in execution. The collection of purified fractions is straightforward because of the flow-elution nature of FFF. As a preparative tool, FFF is shown here to be capable of producing microgram quantities of purified DNA.

It is instructive to compare the potential of different FFF techniques for DNA separation and measurement. Most significant is the fact that different FFF methods separate on the basis of different physicochemical constants. Accordingly, the various FFF techniques taken together are capable of providing measurements of a variety of relevant constants of the separated species. Flow FFF, as noted above, achieves separation on the basis of differences in translational diffusion coefficients; accordingly it is capable of measuring D values. Sedimentation FFF, by contrast, achieves separation based on mass differences, and it has the associated capability of measuring mass or molecular weight. (Electrical FFF, which separates on the basis of charge differences, is not yet well enough developed to be considered as a practical tool for DNA separation.) The separation of linear DNA chains by sedimentation FFF is, in principle, somewhat more selective than that achieved by flow FFF, but it has the disadvantage that the apparatus is more complicated and expensive and that the lower M limit is ~10^6–10^7 Da (compared to ~10^3 for flow FFF) depending upon the upper limit of the rotor speed.

It is interesting to note some special cases subject to one FFF technique but not another. Thus given two double-stranded DNAs of equal chain length, one circular and one linear, sedimentation FFF would be incapable of separation because of their equal mass. These two species could be separated by flow FFF by virtue of their differences in hydrodynamic diameters and thus D values. Similarly, circular DNAs with different numbers of superhelical turns should be separable by flow FFF but not by sedimentation FFF. Conversely, two DNA molecules having different masses but equal hydrodynamic diameters could be separated by sedimentation FFF but not flow FFF. Thus these techniques tend to be complementary in their fractionating capability. They are also complementary in their measurement capability, with sedimentation FFF, as noted above, providing molecular mass measurements and with flow FFF providing diffusion coefficients.

The extension of FFF techniques to longer strands of DNA is a particular challenge. It is likely that applicability can be extended significantly beyond 10^7 Da providing detector sensitivity is enhanced to avoid overloading. However, it is probable that new retention time equations will need to be developed because of the onset of shear-related hydrodynamic forces. With still greater chain lengths it becomes very difficult, as has long been recognized,[99-101] to manipulate DNA in shear flow without risk of chain rupture. Thus these extremely long chains may not be compatible with FFF operation because of its flow and shear basis. However, if simple means can be found to condense DNA into relatively compact particles less subject to shear disruption, as is possible by the application of water-soluble polymers and salts, then FFF would regain its applicability based on the proven capabilities of FFF for the separation of colloidal particles.[78,79]

A major objective of this work has been the acquisition of diffusivity data using flow FFF. Flow FFF appears to have several advantages for such measurements including its speed and experimental convenience, its capability of ridding the desired product of impurities, and the fact that submicrogram quantities are sufficient for measurement. However, the accuracy of flow FFF D measurements has not yet been well documented. Recent results with proteins suggest that diffusion coefficients can be measured

to within about 4.4% of literature values. (Some of the discrepancy might arise from literature errors.) The D values obtained from flow FFF in this paper are shown by Figure 11 to be consistent with the trend of other measured values. While in principle flow FFF measurements should be quite accurate, the dependence of D on w^2 as shown by eq 11 means that great care must be taken in determining the true thickness w of the flow FFF channel. This determination is not always trivial when compressible membranes are used for the accumulation wall of the channel, but new methods for measuring the channel void volume should produce more accurate w values.[60] Also, calibration against standards of known D (such as polystyrene latex beads) can be used. More study is needed to evaluate and further improve the accuracy and speed of D by flow FFF.

Acknowledgment. This work was supported by Grant DE-FG02-89ER60851 from the Department of Energy.

References and Notes

(1) Smith, C. L.; Lawrence, S. K.; Gillespie, G. A.; Cantor, C. R.; Weissman, S. M.; Collins, F. S. In *Methods in Enzymology*; Gottesman, M. M., Ed.; Academic Press: New York, 1987; Vol. 151, pp 461–489.
(2) Van Ommen, G. J. N.; Verkerk, J. M. H. In *Human Genetic Diseases, a Practical Approach*; Davies, K., Ed.; IRL Press: Oxford, U.K., 1986; pp 113–133.
(3) Watson, J. D.; Tooze, J.; Kurtz, D. T. *Recombinant DNA, A Short Course*; W. H. Freeman & Co.: New York, 1983.
(4) Swerdlow, H.; Zhang, J. Z.; Chen, D. Y.; Harke, H. R.; Grey, R.; Wu, S.; Dovichi, N. J.; Fuller, C. *Anal. Chem.* **1991**, *63*, 2835.
(5) Cohen, A. S.; Najarian, D.; Smith, J. A.; Karger, B. L. *J. Chromatogr.* **1988**, *458*, 323.
(6) Schwartz, D. C.; Cantor, C. R. *Cell* **1984**, *37*, 67.
(7) Gardiner, K. *Anal. Chem.* **1991**, *63*, 658.
(8) Freifelder, D. *J. Mol. Biol.* **1970**, *54*, 567.
(9) Kavenoff, R. *J. Mol. Biol.* **1972**, *72*, 801.
(10) Colpan, M.; Riesner, D. *J. Chromatogr.* **1984**, *296*, 339.
(11) Stowers, D. J.; Kiem, J. M. B.; Paul, P. S.; Lyoo, Y. S.; Merion, M.; Benbow, R. M. *J. Chromatogr.* **1988**, *444*, 47.
(12) Giddings, J. C. *J. Chromatogr.* **1976**, *125*, 3.
(13) Giddings, J. C.; Myers, M. N.; Caldwell, K. D.; Fisher, S. R. In *Methods of Biochemical Analysis*; Glick, D., Ed.; John Wiley: New York, 1980; Vol. 26, pp 79–136.
(14) Giddings, J. C. *Sep. Sci. Technol.* **1984**, *19*, 831.
(15) Caldwell, K. D. *Anal. Chem.* **1988**, *60*, 959A.
(16) Giddings, J. C. *Chem. Eng. News* **1988**, *66* (Oct 10), 34.
(17) Giddings, J. C. *Sep. Sci.* **1966**, *1*, 123.
(18) Giddings, J. C.; Karaiskakis, G.; Caldwell, K. D.; Myers, M. N. *J. Colloid Interface Sci.* **1983**, *92*, 66.
(19) Giddings, J. C. *J. Chromatogr.* **1989**, *480*, 21.
(20) Giddings, J. C. *Unified Separation Science*; John Wiley: New York, 1991.
(21) Beckett, R.; Bigelow, J. C.; Zhang, J.; Giddings, J. C. In *Influence of Aquatic Humic Substances on Fate and Treatment of Pollutants*; MacCarthy, P., Suffet, I. H., Eds.; Advances in Chemistry Series 219; American Chemical Society: Washington, DC, 1988; Chapter 5.
(22) Ratanathanawongs, S. K.; Giddings, J. C. In *Particle Size Distribution II: Assessment and Characterization*; Provder, T., Ed.; ACS Symposium Series 472; American Chemical Society: Washington, DC, 1991; Chapter 15.
(23) Kirkland, J. J.; Yau, W. W. *Science* **1982**, *218*, 121.
(24) Schallinger, L. E.; Yau, W. W.; Kirkland, J. J. *Science* **1984**, *225*, 434.
(25) Schallinger, L. E.; Gray, J. E.; Wagner, L. W.; Knowlton, S.; Kirkland, J. J. *J. Chromatogr.* **1985**, *342*, 67.
(26) Kirkland, J. J.; Dilks, C. H., Jr.; Rementer, S. W.; Yau, W. W. *J. Chromatogr.* **1992**, *593*, 339.
(27) Wahlund, K.-G.; Litzén, A. *J. Chromatogr.* **1989**, *461*, 73.
(28) Litzén, A.; Wahlund, K.-G. *J. Chromatogr.* **1989**, *476*, 413.
(29) Giddings, J. C.; Benincasa, M. A.; Liu, M.-K.; Li, P. *J. Liq. Chromatogr.* **1992**, *15*, 1729.
(30) Giddings, J. C.; Yang, F. J.; Myers, M. N. *Anal. Chem.* **1976**, *48*, 1126.
(31) Giddings, J. C.; Yang, F. J.; Myers, M. N. *Science* **1976**, *193*, 1244.
(32) Giddings, J. C.; Yang, F. J.; Myers, M. N. *J. Virol.* **1977**, *21*, 131.
(33) Giddings, J. C.; Yang, F. J.; Myers, M. N. *Anal. Biochem.* **1977**, *81*, 395.
(34) Wahlund, K.-G.; Winegarner, H. S.; Caldwell, K. D.; Giddings, J. C. *Anal. Chem.* **1986**, *58*, 573.
(35) Wahlund, K.-G.; Giddings, J. C. *Anal. Chem.* **1987**, *59*, 1332.
(36) Litzén, A.; Wahlund, K.-G. *Anal. Chem.* **1991**, *63*, 1001.
(37) Kirkland, J. J.; Dilks, C. H., Jr.; Rementer, S. W. *Anal. Chem.* **1992**, *64*, 1295.
(38) Jönsson, J. A.; Carlshaf, A. *Anal. Chem.* **1989**, *61*, 11.
(39) Eisenberg, H. *Acc. Chem. Res.* **1987**, *20*, 276.
(40) Schurr, J. M.; Schmitz, K. S. *Annu. Rev. Phys. Chem.* **1986**, *37*, 271.
(41) Hagerman, P. J. *Annu. Rev. Biophys. Biophys. Chem.* **1988**, *17*, 265.
(42) Cantor, C. R.; Schimmel, P. R. *Biophysical Chemistry*; W. H. Freeman & Co.: New York, 1980.
(43) Bloomfield, V. A.; Crothers, D. M.; Tinoco, I., Jr. *Physical Chemistry of Nucleic Acids*; Harper & Row: New York, 1974; p 171.
(44) Kratky, O.; Porod, G. *Recl. Trav. Chim. Pays-Bas* **1949**, *68*, 1106.
(45) Flory, P. J. *Principles of Polymer Chemistry*; Cornell University Press: Ithaca, NY, 1953.
(46) Kirkwood, J. G.; Riseman, J. *J. Chem. Phys.* **1948**, *16*, 565.
(47) Kam, Z.; Borochov, N.; Eisenberg, H. *Biopolymers* **1981**, *20*, 2671.
(48) Borochov, N.; Eisenberg, H. *Biopolymers* **1984**, *23*, 1757.
(49) Sorlie, S. S.; Pecora, R. *Macromolecules* **1990**, *23*, 487.
(50) Mandelkern, L.; Flory, P. J. *J. Chem. Phys.* **1952**, *20*, 212.
(51) Crothers, D. M.; Zimm, B. H. *J. Mol. Biol.* **1965**, *12*, 525.
(52) Eigner, J.; Doty, P. *J. Mol. Biol.* **1965**, *12*, 549.
(53) Reinert, K. E.; Strassburger, J.; Triebel, H. *Biopolymers* **1971**, *10*, 285.
(54) Tirado, M. M.; Garcia de la Torre, J. *J. Chem. Phys.* **1984**, *81*, 2047.
(55) Yamakawa, H.; Fujii, M. *Macromolecules* **1973**, *6*, 407.
(56) Yamakawa, H.; Stockmayer, W. H. *J. Chem. Phys.* **1972**, *57*, 2843.
(57) Hearst, J. E.; Stockmayer, W. H. *J. Chem. Phys.* **1962**, *37*, 1425.
(58) Fujii, M.; Yamakawa, H. *Macromolecules* **1975**, *8*, 792.
(59) Giddings, J. C.; Chen, X.; Wahlung, K.-G.; Myers, M. N. *Anal. Chem.* **1987**, *59*, 1957.
(60) Giddings, J. C.; Williams, P. S.; Benincasa, M. A. *J. Chromatogr.* **1992**, *627*, 23.
(61) Maniatis, T.; Fritsch, E. F.; Sambrook, J. *Molecular Cloning: A Laboratory Manual*; Cold Spring Harbor Laboratory: Cold Spring Harbor, NY, 1982.
(62) Wilson, D. H.; Price, H. L.; Henderson, J.; Hanlon, S.; Benight, A. S. *Biopolymers* **1990**, *29*, 357.
(63) Karaiskakis, G.; Myers, M. N.; Caldwell, K. D.; Giddings, J. C. *Anal. Chem.* **1981**, *53*, 1314–1317.
(64) Caldwell, K. D.; Brimhall, S. L.; Gao, Y.; Giddings, J. C. *J. Appl. Polym. Sci.* **1988**, *36*, 703.
(65) Hansen, M. E.; Giddings, J. C.; Beckett, R. *J. Colloid Interface Sci.* **1989**, *132*, 300.
(66) Liu, M.-K.; Williams, P. S.; Myers, M. N.; Giddings, J. C. *Anal. Chem.* **1991**, *63*, 2115.
(67) Thompson, D. S.; Gill, S. J. *J. Chem. Phys.* **1967**, *47*, 5008.
(68) Callis, P. R.; Davison, N. *Biopolymers* **1969**, *8*, 379.
(69) Davison, P. F. *Proc. Natl. Acad. Sci. U.S.A.* **1959**, *45*, 1560.
(70) Adam, R. E.; Zimm, B. H. *Nucl. Acid. Res.* **1977**, *4*, 1513.
(71) Odell, J. A.; Muller, A. J.; Narh, K. A.; Keller, A. *Macromolecules* **1990**, *23*, 3092.
(72) Odell, J. A.; Keller, A.; Rabin, Y. *J. Chem. Phys.* **1988**, *88*, 4022.
(73) Lee, S.; Giddings, J. C. *Anal. Chem.* **1988**, *60*, 2328.
(74) DiMarzio, E. A.; Guttman, C. M. *Macromolecules* **1970**, *3*, 131.
(75) Giddings, J. C.; Moon, M. H.; Williams, P. S.; Myers, M. N. *Anal. Chem.* **1991**, *63*, 1366.
(76) Bloomfield, V. A.; Crothers, D. M.; Tinoco, I., Jr. *Physical Chemistry of Nucleic Acids*; Harper & Row: New York, 1974.
(77) Giddings, J. C.; Li, S.; Williams, P. S.; Schimpf, M. E. *Makromol. Chem., Rapid Commun.* **1988**, *9*, 817.
(78) Barman, B. N.; Giddings, J. C. In *Size Exclusion Chromatography, Field-Flow Fractionation, and Related Chromatographic Methods of Polymer Analysis*; Provder, T., Ed.; ACS Symposium Series; American Chemical Society: Washington, DC; in press.
(79) Barman, B. N.; Giddings, J. C. *Langmuir* **1992**, *8*, 51.
(80) Lerman, L. S. *Proc. Natl. Acad. Sci. U.S.A.* **1971**, *68*, 1886.
(81) Riemer, S. C.; Bloomfield, V. A. *Biopolymers* **1978**, *17*, 785.
(82) Post, C. B.; Zimm, B. H. *Biopolymers* **1979**, *18*, 1487.
(83) Bloomfield, V. A. *Biopolymers* **1991**, *31*, 1471.
(84) Laemmli, U. K. *Proc. Natl. Acad. Sci. U.S.A.* **1975**, *72*, 4288.
(85) Langowski, J. *Biophys. Chem.* **1987**, *27*, 263.

(86) Newman, J.; Swinney, H. L.; Berkowitz, S. A.; Day, L. A. *Biochemistry* **1974**, *13*, 4832.
(87) Halsall, H. B.; Schumaker, V. N. *Biochemistry* **1972**, *11*, 4692.
(88) Mandelkern, M.; Elias, J. G.; Eden, D.; Crothers, D. M. *J. Mol. Biol.* **1981**, *152*, 153.
(89) Schmitz, K. S.; Lu, M. *Biopolymers* **1984**, *23*, 797.
(90) Nicolai, T.; Mandel, M. *Macromolecules* **1989**, *22*, 2348.
(91) Strasburger, J.; Reinert, K. E. *Biopolymers* **1973**, *10*, 263.
(92) Chen, F. C.; Yeh, A.; Chu, B. *J. Chem. Phys.* **1977**, *66*, 1290.
(93) Soda, K.; Wada, A. *Biophys. Chem.* **1984**, *20*, 185.
(94) Voordouw, G.; Kam, Z.; Borochov, N.; Eisenberg, H. *Biophys. Chem.* **1978**, *8*, 171.
(95) Sorlie, S. S.; Pecora, R. *Macromolecules* **1988**, *21*, 1437.
(96) Lang, D.; Coates, P. *J. Mol. Biol.* **1968**, *36*, 137.
(97) Schmidt, R. L. *Biopolymers* **1973**, *12*, 1427.
(98) Tanford, J. *Physical Chemistry of Macromolecules*; Wiley: New York, 1961; p 363.
(99) Massie, H. R.; Zimm, B. H. *Proc. Natl. Acad. Sci. U.S.A.* **1972**, *69*, 1188.
(100) Cairns, J. *J. Mol. Biol.* **1963**, *6*, 208.
(101) Klotz, L. C.; Zimm, B. H. *J. Mol. Biol.* **1972**, *72*, 779.